REGULAR ARTICLE

blood advances

Integrin VLA-4 as a PET imaging biomarker of hyper-adhesion in transgenic sickle mice

Lydia A. Perkins,[1,2,*] Lea Nyiranshuti,[2,*] Lynda Little-Ihrig,[1] Joseph D. Latoche,[2] Kathryn E. Day,[2] Qin Zhu,[2] Sina Tavakoli,[1-3] Prithu Sundd,[1,4] Enrico M. Novelli,[1,5,6] and Carolyn J. Anderson[1-4,6,7]

[1]Vascular Medicine Institute, [2]Division of Cardiology, Department of Medicine, [3]Department of Radiology, [4]Department of Bioengineering, [5]Division of Hematology/Oncology, Department of Medicine, [6]Department of Pharmacology and Chemical Biology, and [7]Department of Chemistry, University of Pittsburgh, Pittsburgh, PA

Key Points

- PET imaging of LPS-induced hyper-adhesion revealed focal ^{64}Cu-LLP2A uptake in the humeri and femurs in SCD mice.
- Treatment with an anti-P-selectin mAb prevented LPS-induced focal ^{64}Cu-LLP2A uptake in SCD mice.

In sickle cell disease (SCD), very late antigen-4 (VLA-4 or integrin $\alpha_4\beta_1$) mediates the adhesion of reticulocytes to inflamed, proinflammatory endothelium, a key process in promoting vaso-occlusive episodes (VOEs). We hypothesized that a radionuclide tracer targeting VLA-4 could be harnessed as a positron emission tomography (PET) imaging biomarker of VOEs. We tested the VLA-4 peptidomimetic PET tracer ^{64}Cu-CB-TE1A1P-PEG$_4$-LLP2A (^{64}Cu-LLP2A) for imaging hyper-adhesion–associated VOEs in the SCD Townes mouse model. With lipopolysaccharide (LPS)-induced VOEs, ^{64}Cu-LLP2A uptake was increased in the bone marrow of the humeri and femurs, common sites of VOEs in SCD mice compared with non-SCD mice. Treatment with a proven inhibitor of VOEs (the anti-mouse anti-P-selectin monoclonal antibody [mAb] RB40.34) during LPS stimulation led to a reduction in the uptake of ^{64}Cu-LLP2A in the humeri and femurs to baseline levels, implying blockade of VOE hyper-adhesion. Flow cytometry with Cy3-LLP2A demonstrated an increased percentage of VLA-4–positive reticulocytes in SCD vs non-SCD mice in the bone and peripheral blood after treatment with LPS, which was abrogated by anti-P-selectin mAb treatment. These data, for the first time, show in vivo imaging of VLA-4–mediated hyper-adhesion, primarily of SCD reticulocytes, during VOEs. PET imaging with ^{64}Cu-LLP2A may serve as a valuable, noninvasive method for identifying sites of vaso-occlusion and may provide an objective biomarker of disease severity and anti-P-selectin treatment efficacy in patients with SCD.

Introduction

Sickle cell disease (SCD) is a genetic disorder that affects about 100 000 people in the United States and millions globally, mostly in sub-Saharan Africa.[1,2] The root cause of SCD is the polymerization of deoxygenated hemoglobin S (HbS), which results in the deformation of red blood cells (RBCs) into elongated, sickle-shaped cells. SCD is characterized by hemolysis, cellular hyper-adhesion, chronic inflammation, and painful vaso-occlusive episodes (VOEs).[3] VOEs result in tissue ischemia leading to acute pain and generalized organ dysfunction.[4] Acute pain from VOEs is the most common reason for hospital admission in patients with SCD.[5] A high rate of VOEs is associated with early death in patients who are older than age 20 years and adversely affects quality of life.[6,7] To date, there are no objective, quantifiable biomarkers of VOE, so the diagnosis of VOE exclusively relies on the patient's self-report. Patient-reported outcomes are important, but the lack of objective biomarkers has hampered clinical

Submitted 10 June 2020; accepted 15 July 2020; published online 3 September 2020. DOI 10.1182/bloodadvances.2020002642.

*L.A.P. and L.N. contributed equally to this study as first authors.

For original data, please contact Carolyn J. Anderson (carolyn.j.anderson@missouri.edu) and Enrico M. Novelli (noveex@upmc.edu).

The full-text version of this article contains a data supplement.

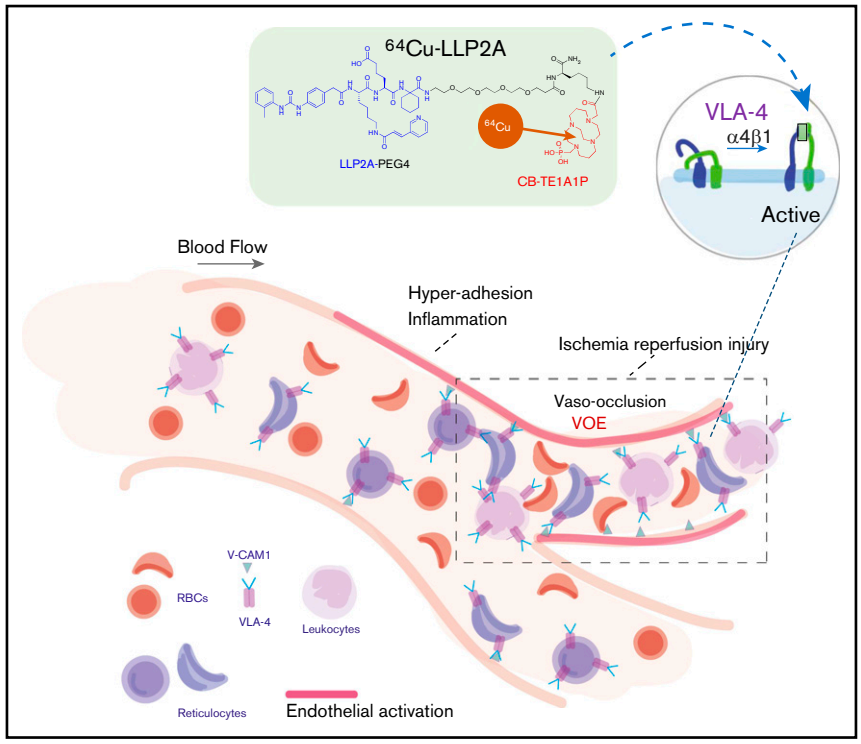

Figure 1. Rationale for PET imaging of VLA-4 as a biomarker of hyper-adhesion. The PET tracer ^{64}Cu-CB-TE1A1P-PEG$_4$-LLP2A binds specifically to the active conformation of VLA-4. VLA-4 is expressed on leukocytes and reticulocytes and contributes to vaso-occlusion.[12-14,41,48]

research. In addition, objective biomarkers are needed to determine the eligibility of and response to the new and emerging drugs to prevent VOEs.

A large body of literature shows that hyper-adhesion of blood cells to the endothelium and to one another is critical to vaso-occlusion.[8] RBC sickling and hemolysis lead to a chronic inflammatory state characterized by overexpression of adhesion molecules on RBCs, leukocytes, platelets, and endothelial cells.[8] In response to various triggers, such as hypoxia and acute infection, acute hyper-adhesion leads to trapping of circulating cells in the microvasculature, and ischemia-reperfusion injury, which further promotes inflammation and hyper-adhesion in a vicious cycle.[8]

The role of selectins, integrins, and immunoglobulin superfamily cellular adhesion molecules in vaso-occlusion has been thoroughly investigated in humanized transgenic sickle mice that express human HbS, and also in in vitro flow fluidics systems.[9-11] Among adhesion molecules, very late antigen-4 (VLA-4), also known as integrin $\alpha_4\beta_1$, is a transmembrane noncovalent heterodimer of integrin α_4 and β_1 (CD49d and CD29, respectively) that has emerged as a significant contributor to adhesion because of its overexpression by sickle reticulocytes.[12-14] VLA-4 mediates the adhesion of reticulocytes to the endothelium via binding to endothelial vascular cell adhesion molecule-1 (VCAM-1) (Figure 1).[15] Multiple lines of evidence implicate VLA-4–mediated adhesion in vaso-occlusion: (1) VCAM-1 plasma levels are increased in the patients most severely affected by SCD and in those with VOEs[16,17]; (2) blockade of VLA-4 by the monoclonal antibody (mAb) natalizumab inhibits >50% of the binding of sickle blood cells to tumor necrosis factor α (TNF-α)–activated human umbilical vein endothelial cell monolayers in a microfluidic system[12]; and (3) treatment with hydroxyurea, which reduces the rate of VOEs, also reduces reticulocyte VLA-4 expression in patients.[18,19] P-selectin is another major player in the hyper-adhesion cascade of vaso-occlusion. Among the selectins, P-selectin is responsible for the tethering and rolling of leukocytes to sites of inflamed endothelium via binding to P-selectin glycoprotein ligand-1 (PSGL-1).[20] P-selectin is also involved in sickle RBC adhesion.[21-24] A randomized clinical trial of the anti-human, anti-P-selectin mAb crizanlizumab in patients with SCD provided the most compelling evidence of the role of P-selectin in VOEs.[25] High-dose crizanlizumab (5 mg/kg), administered via monthly infusions, prevented 45% of VOEs compared with placebo.[25] Furthermore, in a sickle mouse model, anti-P-selectin mAb treatment prevented vaso-occlusion in the lungs.[9] Taken together, these studies show that hyper-adhesion is central to VOEs and that VLA-4 and P-selectin are key mediators of hyper-adhesion.

Herein, we propose to harness the hyper-adhesive state of SCD as a biomarker of VOEs. We hypothesize that positron emission tomography (PET) with a specific tracer for active VLA-4 can noninvasively assess hyper-adhesion specific to vaso-occlusion (Figure 1). Our laboratory has developed the tracer ^{64}Cu-CB-TE1A1P-PEG$_4$-LLP2A (^{64}Cu-LLP2A), which has high affinity for activated VLA-4 in B16F10 melanoma tumor cells (K_d 0.28 $\pm$ 0.03 nM)[26-28] and binds VLA-4–positive immune cells in granulomas in a cynomolgus macaque model of tuberculosis.[29,30] PET imaging with ^{64}Cu-LLP2A is advantageous in its ability to specifically bind to the activated form of VLA-4. The conformational change from low to high affinity mediates its ability to bind the natural ligand VCAM-1 on the endothelium.[31] We investigated the use of ^{64}Cu-LLP2A as a biomarker for VOEs in sickle (SCD) transgenic Townes mice and non-sickle (non-SCD) Townes controls at baseline and post-lipopolysaccharide (LPS) injection, a known trigger of inflammation and VOEs in SCD mice.[8,9,32] We explored the effect of anti-P-selectin mAb treatment in reducing ^{64}Cu-LLP2A uptake to support the role of our imaging strategy as a precision medicine approach to preventing VOEs.

Materials and methods

Mouse model

Homozygous male SCD and non-SCD control Townes mice were obtained from The Jackson Laboratories (Bar Harbor, ME; stock No. 013071). Mice were aged to 5 to 6 months for the experiments. All animal studies were approved by the University of Pittsburgh Institutional Animal Care and Use Committee. All applicable institutional and/ or national guidelines for the care and use of animals were followed.

^{64}Cu-CB-TE1A1P-PEG$_4$-LLP2A and Cy3-LLP2A synthesis

All chemicals were purchased from Sigma-Aldrich (St. Louis, MO) or Fisher Scientific (Waltham, MA), unless otherwise specified. Rink amide 4-methylbenzhydrylamine resin (loading, 0.47 mmol/g) and all fluorenylmethyloxy carbonyl (Fmoc) protected amino acids were purchased from Chem-Impex (Wood Dale, IL). The anti-P-selectin mAb RB40.34 was obtained from a purified hybridoma source and purchased from the antibody engineering and technology core of the University of Virginia, School of Medicine. ^{64}Cu chloride ($t_{1/2}$ = 12.7 hours, β^+; 17.8%, $E_{\beta+max}$ = 656 KeV, β^-, 38.4%, $E_{\beta\text{-}max}$ = 573 KeV) was obtained from Washington University (St. Louis, MO) and the University of Wisconsin (Madison, WI).

CB-TE1A1P-PEG$_4$-LLP2A was purchased from Auspep (Tullamarine, VIC, Australia). ^{64}Cu-labeled CB-TE1A1P-PEG$_4$-LLP2A (^{64}Cu-LLP2A) was prepared as previously described at a radiochemical purity of >98% and molar activity of 57.2 MBq/nmol.[26] Radiolabeling chemistry reaction and purity were monitored by radio-high-performance liquid chromatography (HPLC; Agilent Technologies, Santa Clara, CA) with a Jupiter C18 column (Phenomenex, Torrance, CA). Cy3-LLP2A was prepared as previously described with Cy3-NHS ester (Lumiprobe; Hallandale Beach, FL).[30] Analytical and semipreparative reversed-phase HPLC were performed on a Waters 1525 Binary HPLC pump (Milford, MA) with a Waters 2489 UV-Vis detector.

PET/CT imaging

PET and computed tomography (PET/CT) data were acquired by using a small animal Inveon Preclinical Imaging Station and the PET and CT images were coregistered using Inveon Research Workstation (IRW) software (Siemens Medical Solutions, Knoxville, TN). PET images were reconstructed with an ordered subsets expectation maximizing 3D algorithm, and the standard uptake values (SUVs) were measured using IRW. For measuring SUVs, bone regions of interest (ROI) were drawn by coronal CT of the proximal-to-distal length of the humeri and femurs, and muscle ROI for background SUV was drawn in axial CT in either the hindlimb or forelimb. The mean SUVs of the humeri and femurs were normalized to muscle mean SUV (background) to obtain an SUV ratio (SUVr) value.

Mice were anesthetized with 2% isoflurane for injections and PET/CT imaging. SCD Townes mice (n = 12) and non-SCD control mice (n = 10) were first imaged at baseline, and PET/CT images were acquired at 24 hours after intravenous injection of ^{64}Cu-LLP2A (7.4 MBq [200 μCi] ± 50% per mouse; 57.2 MBq/nmol). After 1 week, all mice were challenged with an intravenous tail injection of LPS at 0.1 μg per kg of body weight to elicit VOEs, as described by Bennewitz et al,[9] in conjunction with injection of ^{64}Cu-LLP2A (7.4 MBq [200 μCi] ± 50%; 57.2 MBq/nmol) per mouse with subsequent PET/CT imaging at 24 hours after LPS injection (Figure 2A). Additional cohorts of SCD mice were imaged at baseline and 1 week after intravenous tail injection of a solution containing 0.1 μg/kg LPS to elicit VOEs, administered simultaneously with either 2.5 μg/g immunoglobulin G (IgG) λ isotype control (n = 6; BioLegend, #401916) or 2.5 μg/g anti-P-selectin mAb clone RB40.34 (n = 8), respectively, along with ^{64}Cu-LLP2A (7.4 MBq [200 μCi] ± 50% per mouse; 57.2 MBq/nmol). PET/CT imaging was performed 24 hours after intravenous injection of the agents (Figure 2B).

CBC

Complete blood count (CBC) analysis was conducted at baseline and after LPS challenge. Blood was collected through the saphenous or submandibular vein under anesthesia and placed in EDTA-coated tubes. Hemoglobin, hematocrit, white blood cell (WBC), neutrophil, and platelet counts were determined by using the VetScan HM5 analyzer (Abaxis, Union City, CA).

Histology and immunofluorescence microscopy

After obtaining PET/CT images 24 hours after LPS injection, all mice from the imaging studies were euthanized, and organs (forelimb, hindlimb, and spleen) were harvested and prepared for histology and immunofluorescence imaging. All organs were fixed in 2% paraformaldehyde. In addition, bones were decalcified in 10% EDTA followed by immersion in 30% sucrose, and then embedded in optimal cutting temperature compound and frozen for cryosectioning. For histology assessment, 6-μm bone sections and 6-μm spleen sections were stained with hematoxylin and eosin. Histology slides were imaged on a TissueGnostics microscope system (Vienna, Austria) with a 10× objective. Bone and spleen sections were labeled with 1:200 immunofluorescent antibody anti-CD49d (BioLegend #103613). Bones were imaged by using an SIM Zeiss Axio Observer.Z1-inverted microscope with Apotome (Oslo, Norway) with a 10× 0.3 numerical aperture (enhanced contract Plan-Neofluar objective), and spleens were imaged with a Nikon confocal microscope with a 20× air objective.

Flow cytometry

Flow cytometry was used to measure the VLA-4 expression of reticulocytes and WBCs 24 hours after the LPS injection (0.1 μg/kg). Mice (non-SCD, n = 3; SCD, n = 3; SCD + anti-P-selectin mAb treatment [2.5 μg/g], n = 6) were euthanized, and bone marrow (humeri and femurs) and whole blood were collected in fluorescence-activated cell sorting (FACS) buffer (1× phosphate-buffered saline, 2 mM EDTA, 2% fetal bovine serum). Bone marrow cell suspension and whole blood underwent standard RBC lysis, which effectively lyses only mature RBCs.[33] Cells were incubated for 30 minutes in FACS buffer with 1:300 of the antibodies against the following antigens: common leukocyte antigen CD45 (a pan-leukocyte marker [BD Biosciences #550994]), the erythroid marker Ter119 (BD Biosciences #557909), the erythroid marker anti-CD71 (BD Biosciences #561936), and 3 ng/μL of Cy3-LLP2A. After labeling washout, cells were 2% paraformaldehyde fixed in FACS buffer and processed on a BD Fortessa flow cytometer (Becton Dickinson, Franklin Lakes, NJ) within 24 hours. FACS data were analyzed using FlowJo software (Becton Dickinson). Reticulocytes were gated based on CD45$^-$ CD71$^+$Ter119$^+$ and then gated for VLA-4$^+$ cells by VLA-4$^+$ vs SSC-A (side scatter area). The percent active VLA-4$^+$ reticulocytes

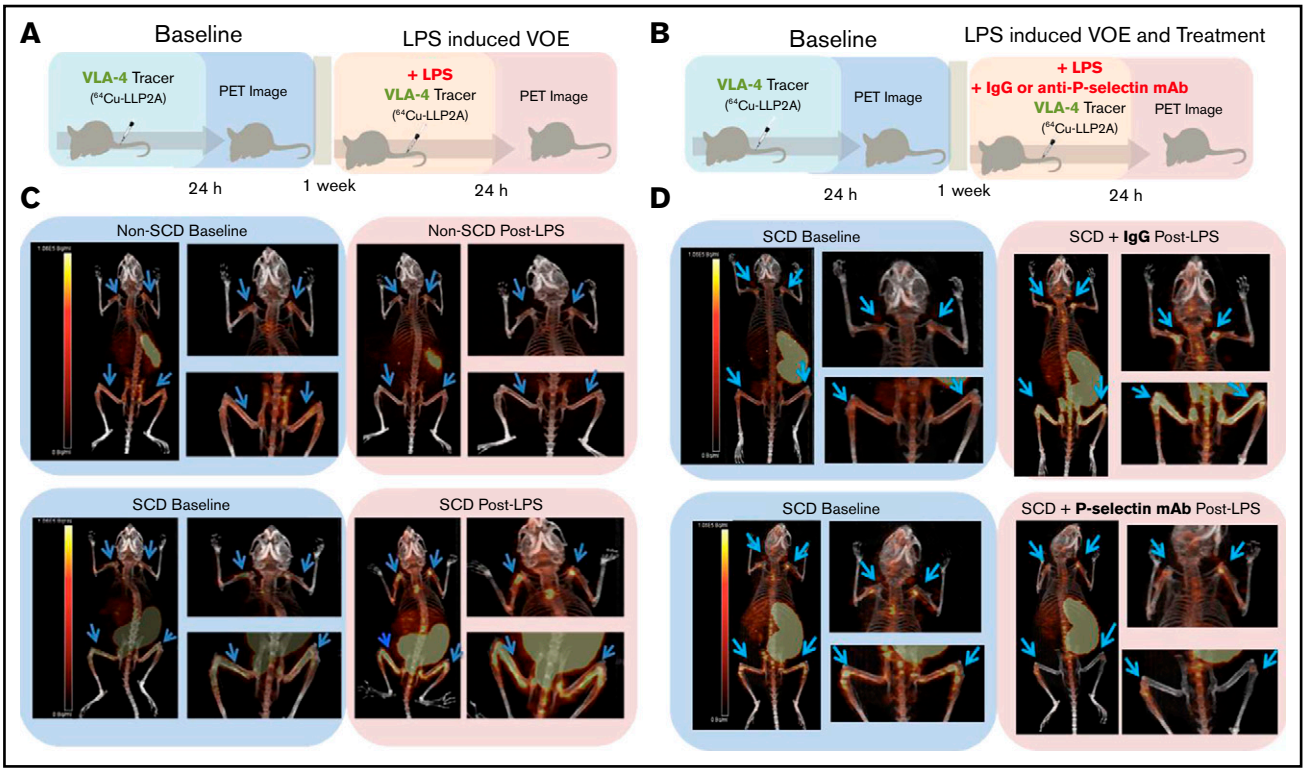

Figure 2. Experimental design and representative PET/CT scans. (A) SCD and non-SCD mice were imaged at baseline, and after 1 week they were injected intravenously with LPS and ^{64}Cu-LLP2A. (B) In a separate set of experiments, mice were imaged at baseline, and after 1 week they were injected intravenously with LPS and either IgG isotype control or anti-P-selectin antibody plus ^{64}Cu-LLP2A. (C) Representative PET/CT images of SCD and non-SCD mice 24 hours after injection of ^{64}Cu-LLP2A at baseline and post-LPS challenge. There are distinct differences between VLA-4 expression in SCD and non-SCD mice post-LPS in the humeri and femurs (blue arrows). (D) Representative PET/CT images of SCD mice 24 hours after injection of ^{64}Cu-LLP2A at baseline and post-LPS with IgG control treatment or anti-P-selectin antibody treatment. Anti-P-selectin treatment mitigates signal in the humeri and femurs (blue arrows) post-LPS.

measurement was based on the VLA-4$^+$ gated subset of the total reticulocyte population (CD45$^-$CD71$^+$Ter119$^+$). WBCs were gated based on CD45$^+$ vs SSC-A, and then gated for VLA-4$^+$ cells by VLA-4$^+$ vs SSC-A. The percent active VLA-4$^+$ WBC measurement was based on the VLA-4$^+$ gated subset of the total WBC population (CD45$^+$). Gating strategies are provided in supplemental Figure 3.

Statistical analysis

Statistical analyses were performed using GraphPad Prism software (San Diego, CA). Statistics are described in each figure legend. $P < .05$ was considered statistically significant. One-way analysis of variance with multiple comparisons was performed by controlling the false discovery rate with the 2-stage linear step-up procedure of Benjamini, Krieger, and Yekutieli.[34] Data are presented as mean ± standard deviation.

Results

^{64}Cu-LLP2A PET/CT shows focal uptake in the humeri and femurs in SCD mice after LPS challenge

At baseline, the mean ^{64}Cu-LLP2A humeri and femurs to muscle SUVr in SCD and non-SCD mice was similar. Post-LPS challenge, the SCD mice showed focal uptake of ^{64}Cu-LLP2A in the humeri and femurs, which are common areas of pain related to vaso-occlusion in humans (Figures 2C and 3; supplemental Figure 1A-B). In SCD mice, the mean humeri SUVr was 5.9 ± 1.5 at baseline and 9.5 ± 1.3 post-LPS challenge ($P < .001$; Figure 3B), whereas the mean femur SUVr was 7.4 ± 1.8 at baseline and 12 ± 3.5 post-LPS challenge ($P < .001$; Figure 3F). Conversely, in non-SCD mice, the mean humeri SUVr was 5.6 ± 0.8 at baseline and 5.1 ± 0.9 post-LPS challenge ($P = .18$; Figure 3A), and the mean femurs:muscle SUVr was 6.6 ± 1.7 at baseline and 6.5 ± 1.8 post-LPS challenge ($P = .78$; Figure 3E). The SCD mice had a significantly greater SUVr fold-change from baseline to post-LPS challenge compared with the non-SCD mice in the humeri (1.7 ± 0.6 vs 0.9 ± 0.2; $P < .001$; Figure 3I) and femurs (1.6 ± 0.3 vs 1.0 ± 0.2; $P < .001$; Figure 3J).

The SCD mice displayed splenomegaly, because the spleen is the major site of extravascular hemolysis and extramedullary hematopoiesis in mice with pathologic conditions.[35] The spleens of both SCD and non-SCD mice showed ^{64}Cu-LLP2A uptake at baseline and post-LPS challenge because splenic stem and progenitor cells express VLA-4.[36,37] Some SCD and non-SCD mice also showed a PET signal in the thymus, a common finding in ^{64}Cu-LLP2A imaging (Figure 2C-D; supplemental Figure 1).[26]

Treatment with an anti-P-selectin mAb prevents LPS-induced focal ^{64}Cu-LLP2A uptake in SCD mice

Next, we tested whether treatment with an anti-P-selectin mAb, a known anti-VOE strategy in humans and Townes mice,[9,38]

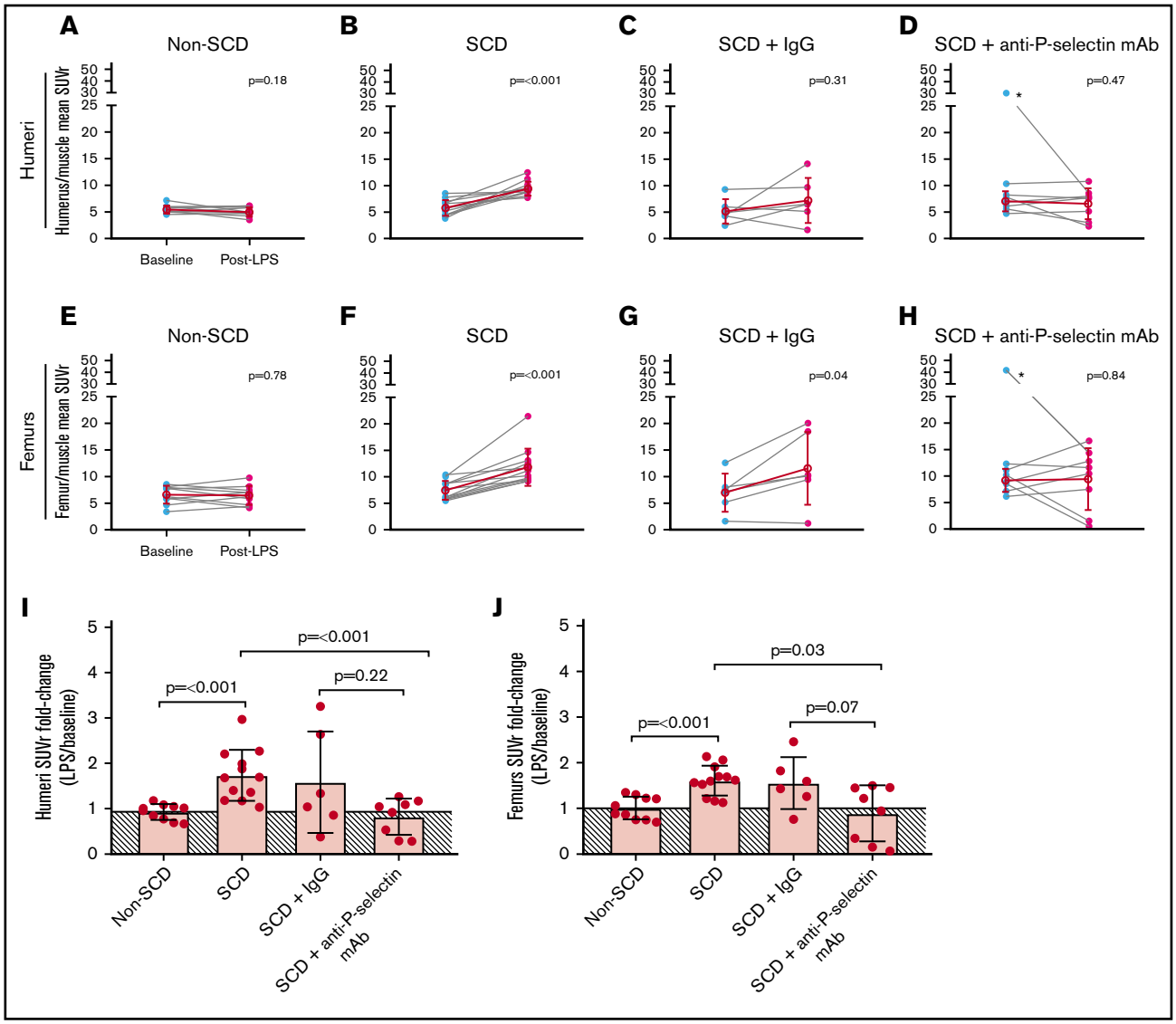

Figure 3. Mean SUVr for humeri and femurs at baseline and post-LPS challenge in non-SCD, SCD, and SCD mice co-treated with LPS and IgG isotype control or anti-P-selectin mAb. (A-D) Mean SUV for humeri divided by mean SUV for muscle for an SUV ratio normalized to background (humeri SUVr) at baseline and post-LPS for non-SCD (A), SCD (B), SCD + IgG isotype control (C), and SCD + anti-P-selectin mAb (D). *Denotes outlier identified by robust regression and outlier removal (ROUT, Q = 1%). (E-H) Mean SUV for femurs divided by mean SUV for muscle for an SUV ratio normalized to background (femurs SUVr) at baseline and post-LPS for non-SCD (E), SCD (F), SCD + IgG isotype control (G), and SCD + anti-P-selectin mAb (H) mice. *Denotes outlier identified by ROUT, Q = 1%. (A-H) Baseline and post-LPS means are shown as a red hollow circle with standard deviation (SD) error bars. Baseline and post-LPS groups were compared by using a paired 2-tailed Student *t* test. $P < .05$ was considered statistically significant. (I-J) SUVr fold-change from baseline to post-LPS (post-LPS/baseline) for humeri and femurs, respectively. The solid line depicts the mean of the non-SCD fold-change (no change, ~1) and is shaded below the threshold. The data were compared using 1-way analysis of variance (ANOVA) with multiple comparisons by controlling false discovery rate (FDR) by a 2-stage linear step-up procedure from Benjamini, Krieger, and Yekutieli. FDR-corrected $P < .05$ was considered statistically significant. ANOVA for humeri and femurs were corrected for unequal variance. (I) Non-depicted *P* values for femurs fold-change: non-SCD vs SCD + IgG ($P = .22$), non-SCD vs SCD + anti-P-selectin mAb ($P = .43$), and SCD vs SCD + IgG ($P = .53$). (J) Non-depicted *P* values for femurs fold-change: non-SCD vs SCD + IgG ($P = .07$), non-SCD vs SCD + anti-P-selectin mAb ($P = .52$), and SCD vs SCD + IgG ($P = .59$).

prevented LPS-induced focal uptake in SCD mice. The humeri mean SUVr was 7.0 ± 1.9 at baseline and 6.6 ± 2.9 post-LPS challenge with the anti-P-selectin mAb ($P = .47$; Figure 3D), whereas the femurs average SUVr was 9.2 ± 2.2 at baseline and 9.4 ± 5.8 post-LPS challenge with the anti-P-selectin mAb ($P = .84$; Figure 3H). These values are consistent with those observed in non-SCD humeri and femurs SUVr at baseline and post-LPS tracer uptake (Figure 3A,E), albeit with more variability. In the SCD mice treated with the anti-P-selectin mAb, the mean SUVr fold-changes (post-LPS challenge/baseline) in the humeri (0.8 ± 0.4) and femurs (0.9 ± 0.6) was significantly smaller than those observed in mice not receiving the anti-P-selectin mAb (1.7 ± 0.6 [$P < .001$] and 1.6 ± 0.3 [$P = .03$], respectively; Figure 3I-J) and were comparable to the change observed in non-SCD mice (0.9 ± 0.2 [$P = .43$] and

1.0 ± 0.2 [P = .52], respectively; Figure 3I-J). In contrast, treatment with an IgG isotype control as a negative control for the anti-P-selectin mAb did not significantly reduce post-LPS challenge/baseline ^{64}Cu-LLP2A uptake in the humeri and femurs (SUVr 1.6 ± 1.1 [P = .53] and 1.6 ± 0.6 [P = .59], respectively; Figure 3I-J).

SCD mice developed significant neutrophilia post-LPS challenge and anti-P-selectin mAb treatments

Hematologic parameters were collected at baseline and post-LPS challenge in SCD and non-SCD control mice (Figure 4; supplemental Table 1). As expected, WBC counts were higher in SCD mice compared with non-SCD mice at baseline and post-LPS challenge (Figure 4A-B,I); however, total WBC counts did not significantly increase after LPS challenge in SCD mice (P = .26; Figure 4B). Treatment with IgG or anti-P-selectin mAb co-administered with LPS also did not significantly alter WBC counts in SCD mice (P = .36 and P = .57, respectively; Figure 4C-D).

SCD mice did not develop leukocytosis (the lymphocyte count, which accounted for the majority of the WBC count, did not change significantly after LPS challenge), but they did develop significant neutrophilia post-LPS challenge compared with non-SCD mice (11 ± 3.8 × 10^9/L and 1.7 ± 1.2 × 10^9/L, respectively; P < .001; Figure 4J). The increase in neutrophil count in SCD mice was further exacerbated by treatment with the anti-P-selectin mAb (14 ± 5.6 × 10^9/L; P = .04; Figure 4J), but there was no baseline to post-LPS increase in the IgG isotype control group (8.0 ± 4.1 × 10^9/L; P = .36; Figure 4G). In support of these data, a similar increase in neutrophil counts was also observed in P-selectin–deficient SCD mice.[39]

Fixed tissue histology and immunofluorescence imaging showed CD49d (integrin α_4) expression in the bone marrow

We evaluated the humeri and femurs of both SCD and non-SCD mice from the PET imaging studies by histology. As expected, given the low dose of LPS we used,[9] samples stained with hematoxylin and eosin showed preserved bone marrow architecture without evidence of infarction. All samples were positive for the α chain of VLA-4 by CD49d labeling, with no appreciable difference between the 2 groups of mice by fluorescence microscopy (supplemental Figure 2), an expected finding because all hematopoietic stem cells express VLA-4.

Treatment with an anti-P-selectin mAb reduces LPS-induced overexpression of activated VLA-4 on reticulocytes

Next, we assessed activated VLA-4 expression on reticulocytes and WBCs by flow cytometry using Cy3-LLP2A, a previously established fluorescent LLP2A conjugate.[28] Specifically, we were interested in measuring the activated VLA-4 expression of reticulocytes and WBCs in the bone marrow and peripheral blood. First, we measured the percent of reticulocytes and WBCs that expressed activated VLA-4 (VLA-4$^+$), and then we measured the average level of expression of VLA-4 in VLA-4$^+$ cells (Figure 5). SCD mice had a higher percentage of VLA-4$^+$ reticulocytes than non-SCD mice in the bone marrow (36 ± 6.5 vs 16 ± 4.2, respectively; P = .002) and blood (38 ± 17 vs 25 ± 6.7, respectively; P = .04; Figure 5A). However, treatment with anti-P-selectin mAb dramatically reduced the percent of LPS-activated VLA-4 reticulocytes in the bone marrow (35 ± 6.5 to 13 ± 6.9; P = .001) and blood (38 ± 17 to 2.4 ± 2.0; P < .001) of SCD mice. In addition, the percent of active VLA-4$^+$ reticulocytes measured in the blood of anti-P-selectin mAb-treated mice was significantly lower compared with that in non-SCD mice (25 ± 6.7; P = .003). Although the percent of VLA-4 active reticulocytes differed between non-SCD, SCD, and SCD mice treated with the anti-P-selectin mAb, the amount of VLA-4 expressed on VLA-4$^+$ reticulocytes was unchanged, as shown by the mean fluorescence intensity (MFI) of Cy3-LLP2A (Figure 5B).

VLA-4$^+$ WBCs presented a more complex profile. The bone marrow from SCD mice had a significantly higher percentage of VLA-4$^+$ WBCs compared with non-SCD mice (43 ± 3.5 and 26 ± 5.6, respectively; P = .007; Figure 5C); however, there was no significant difference in the blood (19 ± 4.0 and 24 ± 6.7, respectively; P = .71). Anti-P-selectin mAb treatment did not significantly change the percentages of VLA-4$^+$ SCD WBCs in the bone marrow (49 ± 8.2; P = .09) or blood (46 ± 19; P = .08). With respect to VLA-4 expression in the VLA-4$^+$ WBCs from the bone marrow, there was no difference between SCD and non-SCD mice (2200 ± 800 and 2200 ± 550 MFI, respectively; P = .91; Figure 5D). There was, however, an almost significant decrease in the average VLA-4 expression of VLA-4$^+$ WBCs after treatment with anti-P-selectin mAb in the bone marrow (910 ± 710 MFI; P = .05; Figure 5D). Interestingly, in blood, we measured significantly lower VLA-4 expression in VLA-4$^+$ WBCs from SCD than from non-SCD mice (Figure 5D). Furthermore, treatment with anti-P-selectin mAb reduced blood VLA-4$^+$ WBCs compared with those in SCD mice receiving LPS without treatment (380 ± 130 and 3200 ± 810 MFI, respectively; P = .002). This observation may be the result of the release of immature neutrophils that express low levels of VLA-4 post-LPS challenge in SCD mice,[40,41] and even more so with anti-P-selectin mAb treatment that increases peripheral neutrophils, lowering the average peripheral VLA-4$^+$ WBC VLA-4 expression with increasing numbers of neutrophils.

Discussion

The discovery of new biomarkers of VOEs to identify patients at risk for specific complications and to monitor treatment responses is a research priority.[42] There remains a paucity of objective findings to diagnose VOEs, which has hampered research and clinical care in SCD.[42,43] In particular, imaging studies of VOEs in humans have been restricted to single-photon emission computerized tomography or magnetic resonance imaging scans of bone marrow infarction,[44-46] a late event that does not always develop during VOEs. Thus, imaging of VOEs has not been routinely incorporated into SCD research or clinical care. Through extensive research on the molecular processes involved in vaso-occlusion, hyper-adhesion has been identified as a critical step in the development of VOEs.[8] In this study, we have shown that imaging of hyper-adhesion by PET with a specific tracer for VLA-4 can noninvasively assess hyper-adhesion specific to vaso-occlusion.

In our experiments, we induced VOEs by injecting a low dose of LPS intravenously, which is adequate to induce vaso-occlusion in SCD mice but innocuous to the control non-SCD mice.[9] Our results showed SCD-specific, focal accumulation of VLA-4 PET signals in the humeri and femurs of SCD mice treated with LPS but not in their

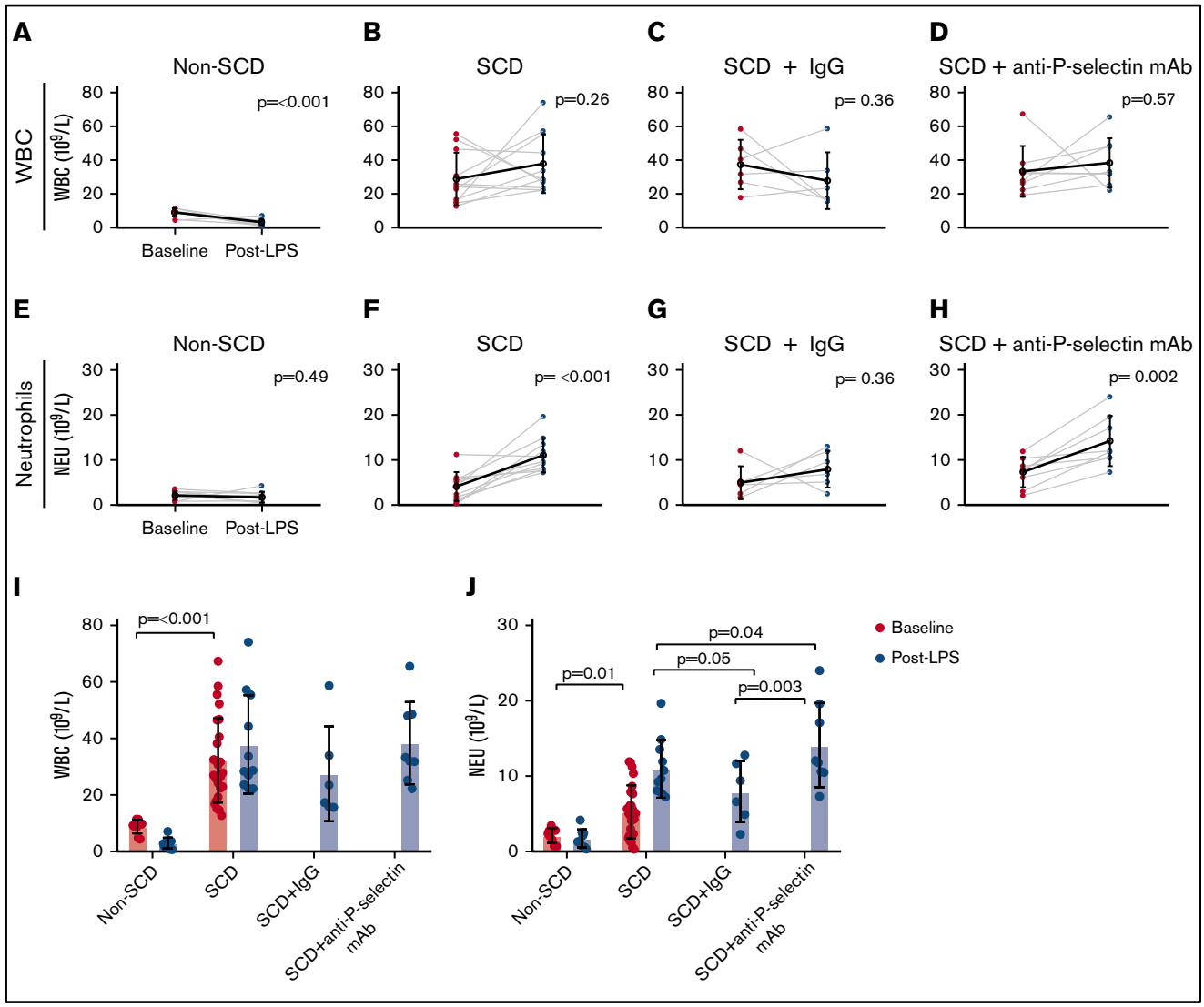

Figure 4. WBC and neutrophil counts for the non-SCD (control), SCD, and SCD mice treated with either IgG isotype control or anti-P-selectin mAb. (A-D) WBC counts ($\times 10^9$/L) at baseline and post-LPS challenge for non-SCD (A), SCD (B), SCD + IgG isotype control (C), and SCD + anti-P-selectin mAb (D). (E-H) Neutrophil (NEU) counts ($\times 10^9$/L) at baseline and post-LPS for non-SCD (E), SCD (F), SCD + IgG isotype control (G), and SCD + anti-P-selectin mAb (H). (A-H) Baseline and post-LPS means are shown as a black hollow circle with SD error bars. Baseline and post-LPS groups were compared using a paired 2-tailed Student *t* test. $P < .05$ was considered statistically significant. (I) Baseline and post-LPS WBC ($\times 10^9$/L) measurements for all conditions. Non-depicted *P* values: post-LPS non-SCD was significantly different from post-LPS SCD ($P \leq .001$), SCD + IgG ($P = .002$), and SCD + anti-P-selectin mAb ($P \leq .001$). (J) Baseline and post-LPS neutrophil ($\times 10^9$/L) measurements for all conditions. Non-depicted *P* values: post-LPS non-SCD was significantly different from post-LPS SCD ($P \leq .001$), SCD + IgG ($P = .002$), and SCD + anti-P-selectin mAb ($P \leq .001$). (I-J) Bars represent mean ± SD. Baseline analysis between SCD and non-SCD used a 2-tailed Student *t* test. One-way ANOVA with multiple comparisons by controlling FDR by a 2-stage linear step-up procedure of Benjamini, Krieger, and Yekutieli was used for the post-LPS analysis. FDR-corrected $P < .05$ was considered statistically significant.

non-SCD controls (Figure 2C; supplemental Figure 1A-B), a finding that indicates that our tracer images SCD-specific hyper-adhesion. The uptake was primarily localized in the joints and long bones of the humeri and femurs—areas of acute pain in individuals with SCD who are experiencing VOEs—thus providing indirect evidence of VLA-4 activity associated with areas of vaso-occlusive pain.

In agreement with the PET results, flow cytometry showed that SCD mice had a larger percentage of active VLA-4$^+$ reticulocytes in the bone marrow and blood compared with non-SCD mice post-LPS challenge (Figure 5B). VLA-4 expression is important for erythroid differentiation and migration from the bone marrow and is normally lost as RBC precursors mature and enter the circulation.[47,48] Reticulocytes from SCD mice are known to maintain surface VLA-4 because of stress erythropoiesis and premature release of VLA-4–expressing reticulocytes into the circulation.[14,49] In our experiments, LPS stimulation increased the proportion of hyper-adhesive VLA-4$^+$ reticulocytes in SCD mice, leading to focal uptake of ^{64}Cu-LLP2A during VOEs.

Treatment with anti-P-selectin has emerged as an important VOE preventive modality in individuals with SCD. In a randomized clinical

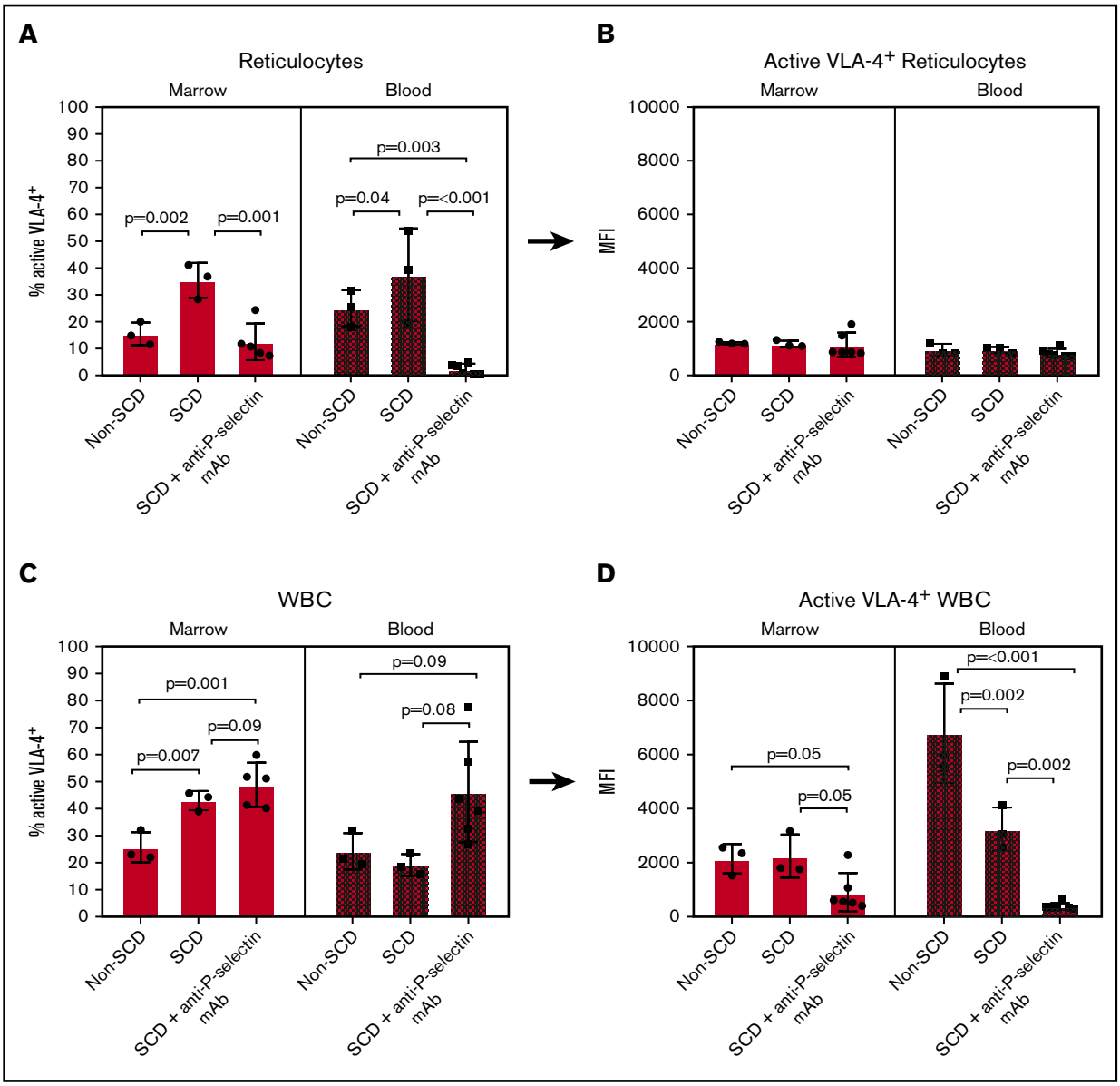

Figure 5. Flow cytometry of isolated bone marrow and blood cells labeled with Cy3-LLP2A post-LPS challenge. (A-B) Reticulocyte-gated measurements. (A) Percent of reticulocytes that express active VLA-4 in the bone marrow and blood. (B) The MFI of Cy3-LLP2A-bound VLA-4 on VLA-4$^+$ reticulocytes. (C-D) WBC-gated measurements. (C) Percent of WBCs that express active VLA-4 in the bone marrow and blood. (D) The MFI of Cy3-LLP2A-bound VLA-4 on VLA-4$^+$ reticulocytes. (A-D) Bars represent mean ± SD. Data were analyzed by 1-way ANOVA with multiple comparisons by controlling FDR by a 2-stage linear step-up procedure of Benjamini, Krieger, and Yekutieli. FDR-corrected $P < .05$ was considered statistically significant.

trial of the anti-P-selectin mAb crizanlizumab vs placebo, patients receiving monthly prophylactic infusions of high-dose crizanlizumab experienced a reduced median per year rate of VOEs of 1.63 compared with 2.98 with placebo (45.3% lower rate; $P = .01$).[25] Presumably, crizanlizumab prevents VOEs by blocking both RBC and WBC interactions with P-selectin on the endothelium.[20-24] Binding to P-selectin is followed by downstream activation and engagement of additional adhesion molecules at sites of vaso-occlusion, including VLA-4. Thus, we tested whether a murine analog of crizanlizumab would prevent VLA-4 activation in our model. We found that an anti-P-selectin mAb administered concurrently with LPS resulted in reduced ^{64}Cu-LLP2A uptake levels that were similar to baseline (Figure 3). The PET findings were mirrored by the results of the flow cytometry analysis that showed a reduction in the percentage of active VLA-4$^+$ reticulocytes in the bone and blood of SCD mice in response to anti-P-selectin mAb treatment (Figure 5A). The flow cytometry studies also demonstrated that the VLA-4$^+$ WBC profiles did not change with anti-P-selectin mAb treatment (Figure 5C-D). In our model, we believe the focal increase in ^{64}Cu-LLP2A uptake post-LPS is primarily the result of VLA-4$^+$ reticulocyte-mediated hyper-adhesion. The mechanism by which treatment with an anti-P-selectin mAb modulates VLA-4 activation on reticulocytes remains to be elucidated. One possible explanation is that anti-P-selectin mAb treatment may reduce systemic inflammation and

expression of the VLA-4 ligand VCAM-1 on the endothelium. Alternatively, treatment with anti-P-selectin mAb may reduce the release of VLA-4^+ reticulocytes from the bone marrow.

As expected, SCD mice developed neutrophilia after LPS challenge (Figure 4); however, we found a surprising increase in neutrophil count after treatment with anti-P-selectin mAb, similar to the findings in P-selectin knockout SCD mice.[39] To our knowledge, CBCs after anti-P-selectin or pan-selectin (rivipansel) mAb treatment in humans and mice have not been reported; therefore, we do not know whether neutrophilia is a common occurrence after treatment with this class of drugs. This finding, if replicated in humans treated with crizanlizumab, may have clinical relevance because neutrophilia is associated with worse outcomes in SCD.[50] We hypothesize that blockade of P-selectin may lead to demargination of neutrophils, a phenomenon similar to corticosteroid-induced neutrophilia.

A limitation of our study is that we did not obtain histologic confirmation of vaso-occlusion in the bone marrow. Direct confirmation of vaso-occlusion in sickle mice is challenging, and typically limited to the finding of vascular congestion with large numbers of sickled RBCs.[51] In a postmortem study of a patient with SCD who died during a VOE, the bone marrow histology showed dilated and engorged small vessels which were not completely occluded by sickled RBCs, a possible fixation artifact.[52] In our experiments, it is likely that restoration of vascular patency and blood flow may have occurred by the time the organs were harvested 24 hours after LPS challenge, a prespecified time point required by our imaging protocol, thus precluding us from detecting earlier microvascular obstructions and their attendant ischemic changes. Future PET assessments and animal euthanasia at earlier time points may circumvent this problem.

In summary, we have demonstrated that ^{64}Cu-LLP2A PET imaging detects VLA-4–mediated hyper-adhesion in SCD mice. The preclinical data presented in this study support translation of ^{64}Cu-LLP2A into clinical studies in patients with SCD. First, ^{64}Cu-LLP2A may introduce a precision medicine approach to SCD care by identifying patients with baseline hyper-adhesion who are more likely to respond to crizanlizumab and by monitoring their response to anti-adhesion therapy. Second, PET imaging may validate the patient's report of pain, help distinguish acute VOEs from chronic pain, and aid in the delivery of care in the challenging arenas of high-dose opioid therapy, discharge planning, and supportive care, where the lack of biomarkers has hampered rational, evidence-based treatment. Third, PET imaging may serve as an objective biomarker of hyper-adhesion in clinical trials, where it could complement subjective and limited outcome measures such as patient-reported pain and rate of hospitalizations for VOEs. Plans are underway to perform ^{64}Cu-LLP2A PET imaging in humans with VOEs to corroborate the link between PET-detected hyper-adhesion and VOE pain.

Acknowledgments

The authors thank Grant Bullock, University of Pittsburgh, for his advice and expertise in flow cytometry.

This work was supported by a University of Pittsburgh, Vascular Medicine Institute grant (P3HVB), by The Pittsburgh Foundation, by a National Institutes of Health (NIH), National Cancer Institute grant (P30CA047904) for shared resources (In Vivo Imaging Facility, The University of Pittsburgh Medical Center Hillman Cancer Center, and by NIH, National Heart, Lung, and Blood Institute training grant (T32 HL129964) (L.A.P.). The University of Pittsburgh, Center of Biologic Imaging provided microscopy access.

Authorship

Contributions: E.M.N. and C.J.A. (principal investigators) conceptualized and designed the study and helped write the manuscript; L.N. produced the PET tracer, participated in the PET imaging experiments, performed image analysis, produced Cy3-LLP2A, and helped write the manuscript; L.A.P. produced the PET tracer, participated in PET imaging experiments, performed image analysis, performed the validation studies for fluorescent microscopy and flow cytometry, and helped write the manuscript; L.L.-I. collected and prepared mouse tissues, helped with all the validation studies, helped interpret the data, and edited the manuscript; J.D.L. performed all mouse injections, drew blood for CBCs, and conducted the PET imaging experiments; K.E.D. conducted the PET imaging experiments and analyzed the images; Q.Z. produced Cy3-LLP2A; S.T. helped analyze and interpret the data and provided critical feedback; and P.S. provided valuable feedback throughout the project, helped interpret the data, and edited the manuscript.

Conflict-of-interest disclosure: The authors declare no competing financial interests.

The current affiliation for L.N. is the Ahmanson Translational Theranostics Division, Department of Molecular and Medical Pharmacology, David Geffen School of Medicine, University of California Los Angeles, Los Angeles, CA.

ORCID profiles: L.A.P., 0000-0001-8814-8090; L.N., 0000-0002-8673-1431; L.L.-I., 0000-0003-3471-2797; S.T., 0000-0003-0574-3914; P.S., 0000-0001-7568-5719; C.J.A., 0000-0002-5663-282X.

Correspondence: Enrico M. Novelli, University of Pittsburgh, E1257 BST, 200 Lothrop St, Pittsburgh, PA 15261; e-mail: emn3@pitt.edu; and Carolyn J. Anderson, University of Missouri, Molecular Imaging and Theranostics Center, 1514 Research Park Dr, Columbia, MO 65211; e-mail: carolyn.j.anderson@missouri.edu.

References

1. Hassell KL. Population estimates of sickle cell disease in the U.S. *Am J Prev Med*. 2010;38(4suppl):S512-S521.
2. Piel FB, Patil AP, Howes RE, et al. Global epidemiology of sickle haemoglobin in neonates: a contemporary geostatistical model-based map and population estimates. *Lancet*. 2013;381(9861):142-151.
3. Novelli EM, Gladwin MT. Crises in sickle cell disease. *Chest*. 2016;149(4):1082-1093.
4. Bender MA. Sickle cell disease. 15 September 2003 (Updated 17 August 2017). In: Adam MP, Ardinger HH, Pagon RA, et al, eds. GeneReviews. Seattle, WA: University of Washington, Seattle; 1993-2020. https://www.ncbi.nlm.nih.gov/books/NBK1377/. Accessed 15 November 2019.

5. Brousseau DC, Owens PL, Mosso AL, Panepinto JA, Steiner CA. Acute care utilization and rehospitalizations for sickle cell disease. *JAMA*. 2010; 303(13):1288-1294.
6. Nagel RL, Fabry ME, Steinberg MH. The paradox of hemoglobin SC disease. *Blood Rev*. 2003;17(3):167-178.
7. Rees DC, Williams TN, Gladwin MT. Sickle-cell disease. *Lancet*. 2010;376(9757):2018-2031.
8. Sundd P, Gladwin MT, Novelli EM. Pathophysiology of sickle cell disease. *Annu Rev Pathol*. 2019;14(1):263-292.
9. Bennewitz MF, Jimenez MA, Vats R, et al. Lung vaso-occlusion in sickle cell disease mediated by arteriolar neutrophil-platelet microemboli. *JCI Insight*. 2017;2(1):e89761.
10. Hidalgo A, Frenette PS. When integrins fail to integrate. *Nat Med*. 2009;15(3):249-250.
11. Kaul DK, Hebbel RP. Hypoxia/reoxygenation causes inflammatory response in transgenic sickle mice but not in normal mice. *J Clin Invest*. 2000;106(3): 411-420.
12. White J, Krishnamoorthy S, Gupta D, et al. VLA-4 blockade by natalizumab inhibits sickle reticulocyte and leucocyte adhesion during simulated blood flow. *Br J Haematol*. 2016;174(6):970-982.
13. Joneckis CC, Ackley RL, Orringer EP, Wayner EA, Parise LV. Integrin alpha 4 beta 1 and glycoprotein IV (CD36) are expressed on circulating reticulocytes in sickle cell anemia. *Blood*. 1993;82(12):3548-3555.
14. Swerlick RA, Eckman JR, Kumar A, Jeitler M, Wick TM. Alpha 4 beta 1-integrin expression on sickle reticulocytes: vascular cell adhesion molecule-1-dependent binding to endothelium. *Blood*. 1993;82(6):1891-1899.
15. Lancelot M, White J, Sarnaik S, Hines P. Low molecular weight heparin inhibits sickle erythrocyte adhesion to VCAM-1 through VLA-4 blockade in a standardized microfluidic flow adhesion assay. *Br J Haematol*. 2017;178(3):479-481.
16. Duits AJ, Pieters RC, Saleh AW, et al. Enhanced levels of soluble VCAM-1 in sickle cell patients and their specific increment during vasoocclusive crisis. *Clin Immunol Immunopathol*. 1996;81(1):96-98.
17. Dworkis DA, Klings ES, Solovieff N, et al. Severe sickle cell anemia is associated with increased plasma levels of TNF-R1 and VCAM-1. *Am J Hematol*. 2011;86(2):220-223.
18. Styles LA, Lubin B, Vichinsky E, et al. Decrease of very late activation antigen-4 and CD36 on reticulocytes in sickle cell patients treated with hydroxyurea. *Blood*. 1997;89(7):2554-2559.
19. Odièvre M-H, Bony V, Benkerrou M, et al. Modulation of erythroid adhesion receptor expression by hydroxyurea in children with sickle cell disease. *Haematologica*. 2008;93(4):502-510.
20. Moore KL, Patel KD, Bruehl RE, et al. P-selectin glycoprotein ligand-1 mediates rolling of human neutrophils on P-selectin. *J Cell Biol*. 1995;128(4): 661-671.
21. Matsui NM, Borsig L, Rosen SD, Yaghmai M, Varki A, Embury SH. P-selectin mediates the adhesion of sickle erythrocytes to the endothelium. *Blood*. 2001;98(6):1955-1962.
22. Embury SH, Matsui NM, Ramanujam S, et al. The contribution of endothelial cell P-selectin to the microvascular flow of mouse sickle erythrocytes in vivo. *Blood*. 2004;104(10):3378-3385.
23. Matsui NM, Varki A, Embury SH. Heparin inhibits the flow adhesion of sickle red blood cells to P-selectin. *Blood*. 2002;100(10):3790-3796.
24. Hebbel RP. Adhesion of sickle red cells to endothelium: myths and future directions. *Transfus Clin Biol*. 2008;15(1-2):14-18.
25. Ataga KI, Kutlar A, Kanter J, et al. Crizanlizumab for the prevention of pain crises in sickle cell disease. *N Engl J Med*. 2017;376(5):429-439.
26. Beaino W, Anderson CJ. PET imaging of very late antigen-4 in melanoma: comparison of 68Ga- and 64Cu-labeled NODAGA and CB-TE1A1P-LLP2A conjugates. *J Nucl Med*. 2014;55(11):1856-1863.
27. Beaino W, Nedrow JR, Anderson CJ. Evaluation of (68)Ga- and (177)Lu-DOTA-PEG4-LLP2A for VLA-4-Targeted PET Imaging and Treatment of Metastatic Melanoma. *Mol Pharm*. 2015;12(6):1929-1938.
28. Choi J, Beaino W, Fecek RJ, et al. Combination treatment of VLA-4 targeted radionuclide therapy and immunotherapy in a mouse model of melanoma. *J Nucl Med*. 2018;59(12):1843-1849.
29. Walrath JR, Silver RF. The $\alpha 4\beta 1$ integrin in localization of Mycobacterium tuberculosis-specific T helper type 1 cells to the human lung. *Am J Respir Cell Mol Biol*. 2011;45(1):24-30.
30. Mattila JT, Beaino W, Maiello P, et al. Positron emission tomography imaging of Macaques with tuberculosis identifies temporal changes in granuloma glucose metabolism and integrin $\alpha 4\beta 1$-expressing immune cells. *J Immunol*. 2017;199(2):806-815.
31. Chigaev A, Sklar LA. Aspects of VLA-4 and LFA-1 regulation that may contribute to rolling and firm adhesion. *Front Immunol*. 2012;3:242.
32. Belcher JD, Chen C, Nguyen J, et al. Heme triggers TLR4 signaling leading to endothelial cell activation and vaso-occlusion in murine sickle cell disease. *Blood*. 2014;123(3):377-390.
33. Schreier S, Borwornpinyo S, Udomsangpetch R, Triampo W. An update of circulating rare cell types in healthy adult peripheral blood: findings of immature erythroid precursors. *Ann Transl Med*. 2018;6(20):406.
34. Benjamini Y, Krieger AM, Yekutieli D. Adaptive linear step-up procedures that control the false discovery rate. *Biometrika*. 2006;93(3):491-507.
35. Nguyen J, Abdulla F, Chen C, et al. Phenotypic characterization the Townes sickle mice [abstract]. *Blood*. 2014;124(21). Abstract 4916.
36. Rettig MP, Ansstas G, DiPersio JF. Mobilization of hematopoietic stem and progenitor cells using inhibitors of CXCR4 and VLA-4. *Leukemia*. 2012;26(1): 34-53.

37. Mazo IB, Massberg S, von Andrian UH. Hematopoietic stem and progenitor cell trafficking. *Trends Immunol*. 2011;32(10):493-503.

38. Ghosh S, Flage B, Weidert F, Ofori-Acquah SF. P-selectin plays a role in haem-induced acute lung injury in sickle mice. *Br J Haematol*. 2019;186(2): 329-333.

39. Bennewitz MF, Tutuncuoglu E, Gudapati S, et al. P-selectin-deficient mice to study pathophysiology of sickle cell disease. *Blood Adv*. 2020;4(2): 266-273.

40. Petty JM, Lenox CC, Weiss DJ, Poynter ME, Suratt BT. Crosstalk between CXCR4/stromal derived factor-1 and VLA-4/VCAM-1 pathways regulates neutrophil retention in the bone marrow. *J Immunol*. 2009;182(1):604-612.

41. Canalli AA, Proença RF, Franco-Penteado CF, et al. Participation of Mac-1, LFA-1 and VLA-4 integrins in the in vitro adhesion of sickle cell disease neutrophils to endothelial layers, and reversal of adhesion by simvastatin. *Haematologica*. 2011;96(4):526-533.

42. Kalpatthi R, Novelli EM. Measuring success: utility of biomarkers in sickle cell disease clinical trials and care. *Hematology Am Soc Hematol Educ Program*. 2018;2018:482-492.

43. Ballas SK. The sickle cell painful crisis in adults: phases and objective signs. *Hemoglobin*. 1995;19(6):323-333.

44. Milner PF, Brown M. Bone marrow infarction in sickle cell anemia: correlation with hematologic profiles. *Blood*. 1982;60(6):1411-1419.

45. Rao S, Solomon N, Miller S, Dunn E. Scintigraphic differentiation of bone infarction from osteomyelitis in children with sickle cell disease. *J Pediatr*. 1985; 107(5):685-688.

46. Cerci SS, Suslu H, Cerci C, et al. Different findings in Tc-99m MDP bone scintigraphy of patients with sickle cell disease: report of three cases. *Ann Nucl Med*. 2007;21(5):311-314.

47. Yanai N, Sekine C, Yagita H, Obinata M. Roles for integrin very late activation antigen-4 in stroma-dependent erythropoiesis. *Blood*. 1994;83(10): 2844-2850.

48. Gee BE, Platt OS. Sickle reticulocytes adhere to VCAM-1. *Blood*. 1995;85(1):268-274.

49. Alon R, Kassner PD, Carr MW, Finger EB, Hemler ME, Springer TA. The integrin VLA-4 supports tethering and rolling in flow on VCAM-1. *J Cell Biol*. 1995;128(6):1243-1253.

50. Hanson MS, Wandersee NJ, Hessner M, et al. Neutrophil activation in sickle cell disease: Biochemical and functional changes at baseline and during acute vaso-occlusive crises [abstract]. *Blood*. 2013;122(21). Abstract 992.

51. Novelli EM, Little-Ihrig L, Knupp HE, et al. Vascular TSP1-CD47 signaling promotes sickle cell-associated arterial vasculopathy and pulmonary hypertension in mice. *Am J Physiol Lung Cell Mol Physiol*. 2019;316(6):L1150-L1164.

52. Athanasou NA, Hatton C, McGee JO, Weatherall DJ. Vascular occlusion and infarction in sickle cell crisis and the sickle chest syndrome. *J Clin Pathol*. 1985;38(6):659-664.